European Polymer Journal 170 (2022) 111165

Contents lists available at ScienceDirect

European Polymer Journal

journal homepage: www.elsevier.com/locate/europolj

Varying the sequence distribution and hydrogen bonding strength provides highly Heat-Resistant PMMA copolymers

Wei-Ting Du [a], Shiao-Wei Kuo [a,b,*]

[a] Department of Materials and Optoelectronic Science, Center of Functional Polymers and Supramolecular Materials, National Sun Yat-Sen University, Kaohsiung 80424, Taiwan

[b] Department of Medicinal and Applied Chemistry, Kaohsiung Medical University, Kaohsiung 807, Taiwan

ARTICLE INFO

Keywords:
Hydrogen bonding
Sequence distribution
PMMA copolymer
FTIR
Thermal property

ABSTRACT

In this study we used free radical copolymerization of methyl methacrylate (MMA) and *N*-hydroxyphenylmaleimide (HPMI) to synthesize various poly(methyl methacrylate–*co*–*N*-hydroxyphenylmaleimide) (PMMA-*co*-PHPMI) random copolymers possessing high glass transition temperatures (T_g). FTIR and NMR spectroscopy, mass spectrometry, and differential scanning calorimetry (DSC) confirmed the chemical structures, thermal properties, hydrogen bonding interactions, and sequence distributions of these random copolymers. Because the reactivity ratio of MMA and HPMI is very different from that of MMA and maleic anhydride (MA), which prefer to form homopolymers, here we obtained partially alternating copolymers featuring strong intermolecular hydrogen bonding between the PMMA and PHPMI segments, resulting in the value of T_g increasing by up to 90 °C relative to that of the pure PMMA homopolymer. In addition, solid state NMR spectra revealed single values for the proton spin–lattice relaxation time in the rotating frame [$T_{1\rho}$(H)] over all compositions of these random copolymers, with the relaxation times being shorter than the predicted average, indicating that the free volume had decreased and that the copolymers possessed rigid structures with high values of T_g.

1. Introduction

Poly(methyl methacrylate) (PMMA) is an optically transparent organic polymeric material that is used widely in optical fibers, compact discs, solar cells, and light guide plates because of its resistance against weathering corrosion, impressive optical properties, and insulating characteristics [1–5]. Nevertheless, PMMA homopolymers possess relatively low glass transition temperatures (T_g, ca. 100–125 °C) when compared with other optical organic materials [e.g., polycarbonate (PC) and cyclic olefin copolymer (COC)]. Many rigid and bulky monomers have been added for random copolymerization to increase the value of T_g and overcome the problems of miscibility and phase separation encountered with polymer blend approaches [6–14]. Because of poor specific interactions among these segments, however, the values of T_g of these resulting random copolymers containing only rigid monomers have generally been lower than those predicted by Fox or linear rules [13,14].

We have previously developed another way to increase the T_g values of PMMA through random copolymerization with hydrogen bond donor units. For example, the methacrylamide (MAAM) monomer forms PMMA-*co*-PMAAM random copolymers in which strong hydrogen bonding occurs in these two segments [15–18]. The random copolymers generally possess values of T_g higher than corresponding binary polymer blends because of a lower degree of rotational freedom, arising from an intramolecular screening effect and the functional group spacing, based on a correlation hole effect [19]. Furthermore, we have also reported the sequence distribution effect of poly(vinyl phenol) (PVPh) with PMMA segments, forming PVPh-*b*-PMMA diblock copolymers and PVPh-*r*-PMMA random copolymers, synthesized through anionic polymerization and free radical copolymerization, respectively [20–23]. We found that the T_g values of these two copolymers were higher than corresponding PVPh/PMMA binary blends at the same PMMA composition, because different fractions of hydrogen-bonded C = O groups of PMMA would be expected as a result of variations in the degrees of rotational freedom. In addition we found that the inter-association equilibrium constant (K_A) of the random copolymer was larger than that of the block copolymer due to an intramolecular screening effect [20]. Furthermore, the sequence distributions of the hydrogen-bonded copolymers played

* Corresponding author at: Department of Materials and Optoelectronic Science, Center of Functional Polymers and Supramolecular Materials, National Sun Yat-Sen University, Kaohsiung 80424, Taiwan.
E-mail address: kuosw@faculty.nsysu.edu.tw (S.-W. Kuo).

https://doi.org/10.1016/j.eurpolymj.2022.111165
Received 17 February 2022; Received in revised form 17 March 2022; Accepted 24 March 2022
Available online 28 March 2022

an important role in determining their values of T_g; we might expect that an alternative sequence distribution would feature stronger intermolecular hydrogen bonding and higher values of T_g when compared with the block and random sequence distributions [20].

An alternating copolymer comprises two different repeat units arranged alternately in the polymer chain. Regularity in the repetition of the structural units is possible only if two monomers M_1 and M_2 are unable to homopolymerize or have a strong preference to react with each other (quasi alternating copolymer). In the theory of copolymerization, a co-monomer pair whose monomer reactivity ratios (r) are almost zero would form an alternating copolymer; for example, $r_1 = r_2 \approx 0$, where $r_1 = k_{11}/k_{12}$ and $r_2 = k_{22}/k_{21}$ with k_{xy} being the reaction constants [24]. For example, alternating copolymers can be synthesized from styrene and maleic anhydride (MA) because their values of r_1 (0.05) and r_2 (0.005) are both close to zero [24]. In contrast, the distinct reactivity ratios of methyl methacrylate (MMA) and MA ($r_1 = 3.4$; $r_2 = 0.01$) imply that the PMMA homopolymer is formed preferably during attempts at copolymerization [24]. To obtain a high ratio of the alternating sequence of hydrogen bonded donor monomers with MMA, in this study we modified the MA monomer in the form of *N*-hydroxyphenylmaleimide (HPMI) [25] and subjected it to free radical copolymerization with MMA to form partially alternating PMMA-*co*-PHPMI copolymers (Fig. 1(A)). The side chains of PHPMI present phenolic OH units formed hydrogen bonds with the side-chain C = O groups of PMMA; we characterized these interactions using Fourier transform infrared (FTIR) and solid state nuclear magnetic resonance (NMR) spectroscopy, because the stretching of the C = O groups and their chemical environment are strongly affected by intermolecular interactions [26–35].

We further used mass-analyzed laser desorption/ionization time-of-flight (MALDI-TOF) mass spectrometry, DSC, and measurements of $T_{1\rho}$(H) values, based on solid-state NMR spectroscopy, to examine the chemical structures, sequence distributions, thermal properties, and domain sizes of these PMMA-*co*-PHPMI copolymers. To investigate the differences in the composition heterogeneity effects of these random copolymers and corresponding binary blends of PMMA and PHPMI, we used solution casting to also prepare binary PMMA/PHPMI blend systems and subjected them to DSC analyses.

2. Experimental section

2.1. Materials

Phosphorus oxide (98%), 4-aminophenol (99%), and MA (98%) were purchased from Sigma–Aldrich. MMA (99%), azobisisobutyronitrile (AIBN), and *p*-toluenesulfonic acid monohydrate (*p*-TsOH·H_2O) were purchased from Showa. *N*,*N*-Dimethylformamide (DMF), sulfuric acid (96%), methanol (MeOH), tetrahydrofuran (THF), toluene, and diethyl ether (Et_2O) were purchased from Acros Organic. The synthesis of HPMI has been described previously [25].

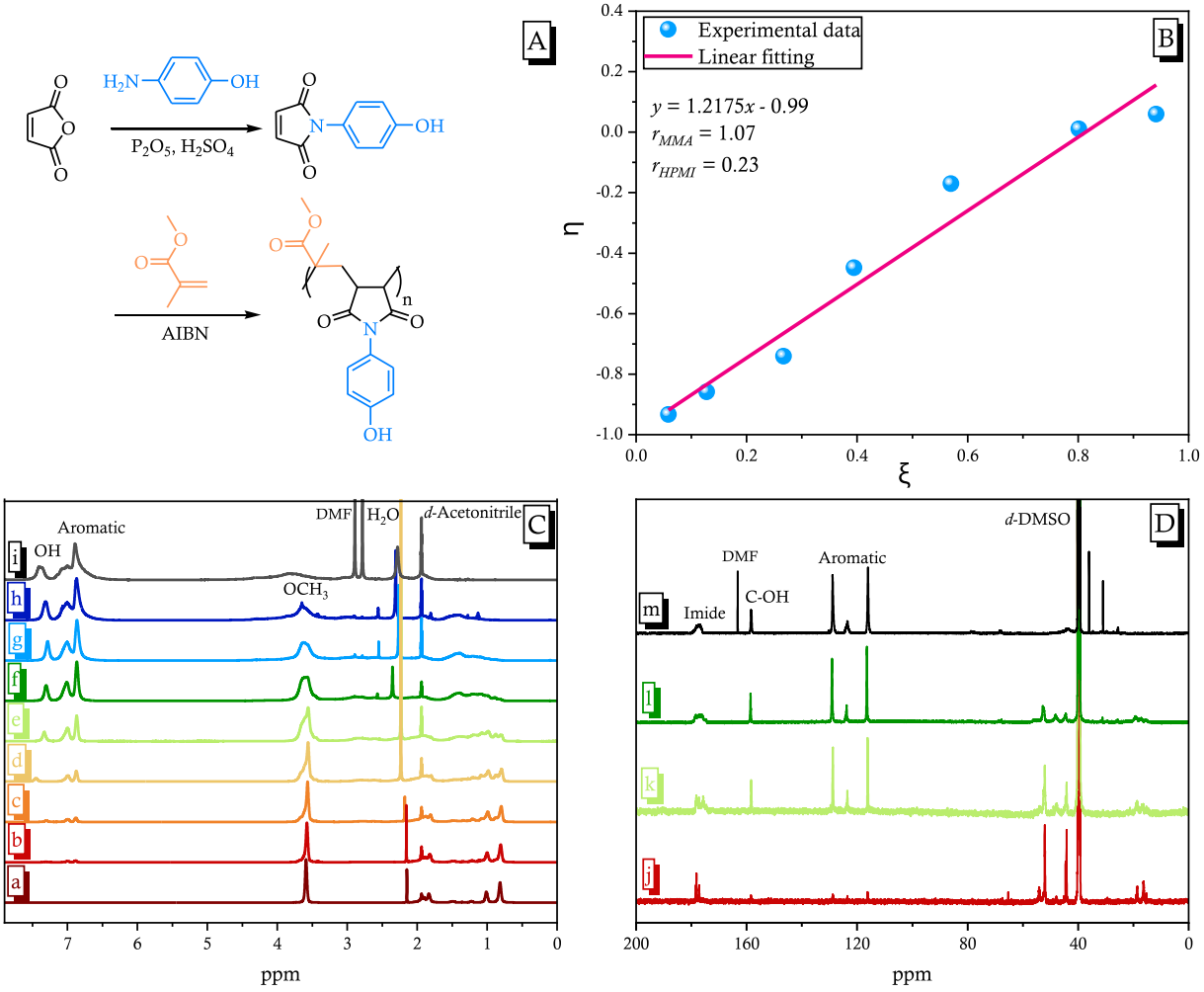

Fig. 1. (A) Synthesis of the HPMI monomer and random copolymerization of PMMA-*co*-PHPMI. (B) Kelen–Tudos plot of the PMMA-*co*-PHPMI copolymers. (C) ^{1}H NMR spectra of (a) pure PMMA, (b) PHPMI-5, (c) PHPMI-10, (d) PHPMI-17, (e) PHPMI-28, (f) PHPMI-41, (g) PHPMI-50, (h) PHPMI-56, and (i) PHPMI. (D) ^{13}C NMR spectra of (j) PHPMI-5, (k) PHPMI-28, (l) PHPMI-41, and (m) PHPMI.

2.2. PMMA/PHPMI binary blends

Various binary PMMA/PHPMI blends were prepared through solution-casting·THF solutions containing 10 wt% binary blend mixtures were stirred for 24 h and then cast onto Teflon dishes. The THF solvent was slowly evaporated at 25 °C for 2 days and then the samples were dried at 50 °C for 3 days.

2.3. PMMA-co-PHPMI random copolymers

A solution of HPMI and MMA (various ratios) in dry THF (50 mL) was stirred in a 100-mL flask at 70 °C under N_2 for 24 h with AIBN as an initiator (5 wt%). The resulting solution was poured into cold Et_2O (1000 mL). The solid precipitate was subjected to many cycles of re-dissolving in cold THF and re-precipitating into Et_2O. The copolymer was dried at 50 °C for 3 days under high vacuum to remove any residual THF. Poly(MMA-*co*-HPMI): FTIR (KBr, cm^{-1}): 1702–1730 (C = O of PMMA and HPMI), 3450 (O–H); ^{1}H NMR (500 MHz, CD_3CN, δ, ppm): 3.40–3.80 (s, 3H, OCH_3), 6.80–7.20 (m, 4H, ArH), 7.20–7.50 (s, 1H, OH); ^{13}C NMR (125 MHz, DMSO-d_6, δ, ppm): 51.40–53.20 (OCH_3), 114.80–130.10 (Ar**C**H), 157.50–159.10 (COH), 173.60–179.70 (NC = O).

3. Results and discussion

3.1. Synthesis of PMMA-co-PHPMI copolymers

We synthesized various PMMA-*co*-PHPMI copolymers through free radical copolymerization of MMA and HPMI [Fig. 1(A)]. We used FTIR, NMR, and MALDI-TOF mass spectrometry to confirm the chemical structures and compositions of these PMMA-*co*-PHPMI random copolymers. Figure S1 reveals that their FTIR spectra were similar to that of the HPMI monomer [25], with a strong absorption for the C = O units at 1702 cm^{-1}, except that broadening of these absorptions occurred after copolymerization with MMA, suggesting the possibility of intermolecular or intramolecular hydrogen bonding. Fig. 1(C) and 1(D) display the ^{1}H and ^{13}C NMR spectra of these PMMA-*co*-PHPMI random copolymers. In the ^{1}H NMR spectrum of the pure PMMA homopolymer, signals appeared at 0.81 and 1.94 ppm for the main-chain CH_2 and CH_3 units and at 3.60 ppm for the side-chain OCH_3 units. For the pure PHPMI homopolymer, signals appeared for the aromatic protons at 6.50–7.20 ppm and for the phenolic OH units at 7.40 ppm. The signals of the OCH_3 units of PMMA and phenolic OH units of PHPMI became broader and shifted downfield after random copolymerization, consistent with intermolecular hydrogen bonding between the PMMA and PHPMI segments. The selected ^{13}C NMR spectra of PMMA-*co*-PHPMI copolymers featured signals at 173.0–179.5 and 158.3 ppm, representing the C = O units of the imide groups and the COH units of the phenolic groups, respectively; signals for the aromatic carbon nuclei appeared at 115.7–129.1 ppm. The FTIR, ^{1}H and ^{13}C NMR spectra confirmed the success of the syntheses of the PMMA-*co*-PHPMI random copolymers. Furthermore, we determined the composition of PHPMI in each copolymer from the peak ratio ($\boldsymbol{A}_{aromatic}/4$)/($\boldsymbol{A}_{aromatic}/4 + \boldsymbol{A}_{OCH3}/3$), based on the signals at 6.50–7.20 and 3.60 ppm [Fig. 1(C)]. Table 1 summarizes the feed ratio of the HPMI monomer and the composition of each resultant PHPMI copolymer, as measured using ^{1}H NMR spectroscopy. The Kelen and Tudos method was used to calculate the reactivity ratios for MMA and HPMI, where $r_1 = k_{11}/k_{12}$ and $r_2 = k_{22}/k_{21}$ are the ratios of the homo/cross propagation rate constants for each monomer, as we have discussed widely in previous reports [36].

$$\eta = \left(r_1 + \frac{r_2}{\alpha}\right)\xi - \frac{r_2}{\alpha} \quad (1)$$

To minimize errors arising from changes in the feed ratio, the monomer conversion should be less than 10% for all copolymerizations. The calculated values of r_{PMMA} (1.07) and r_{PHPMI} (0.23) [Fig. 1(B)] and the apparent linear relationship indicate that the random copolymerizations of these two monomers obeyed a simple terminal model. In addition, the reactivity ratio product ($r_{PMMA} \times r_{PHPMI} = 0.24$) was located in the range 0.18–0.25, suggesting that these copolymers were essentially random distributed, but with a slight tendency toward an alternating distribution [20].

To examine the sequence distributions of these PMMA-*co*-PHPMI copolymers, Fig. 2 presents their corresponding chemical structures, molecular weights [Fig. 2(A)], and MALDI-TOF mass spectra [Fig. 2(B)–2(D)]. We observed evidence for these copolymers featuring partial alternating sequences with equal numbers of MMA and HPMI units [37-39]. As displayed in Fig. 2(B) for PHPMI-41, the difference between the signals at *m/z* 2021.88 and 2312.03 was approximately 289 g mol^{-1}, equal to the summed molecular weight of one MMA unit and one HPMI unit. Fig. 2(C) and 2(D) give similar results, with the differences between *m/z* 2844.79 and 3134.68 for PHPMI-17 and *m/z* 2853.58 and 3144.30 for PHPMI-10 are both approximately 289 g mol^{-1}. Furthermore, there were seven units of both MMA (7 × 100.12 u) and HPMI (7 × 189.17 u) (labeled 7:7) constituting the intense peak at *m/z* 2021.88 in Figure S2 (D), with other obvious peaks in the spectrum of PHPMI-41 corresponding to perfectly alternating sequences with MMA:HPMI ratios of *n*:*n* + 1, *n* + 1:*n*, and *n* + 1:*n* + 1 (e.g., 7:8, 8:7, and 8:8) [37]. Here, we need to emphasize that we assume all these ratios such as 7:7, 7:8, 8:7 and 8:8, corresponding to the alternative sequence distribution because of the low reactivity ratios for both two monomers ($r_{PMMA} \times r_{PHPMI} = 0.24$). A few peaks appeared corresponding to ratios of MMA:HPMI of *n*–2:*n* + 1, *n* + 2:*n*–1, *n* + 4:*n*–2, and *n* + 6:*n*–3 (e.g., 5:8, 9:6, 11:5, and 13:4), arising from homo-polymerization of MMA and HPMI units, with 76.1% of alternating segments. The similar phenomenon was also evident in the spectrum of PHPMI-17 in Figure S2(F), with an intense peak at *m/z* 2844.79 (labeled 19:5), constituting 19 units of MMA (19 × 100.12 u) and five units of HPMI (5 × 189.17 u), as well as 20:5 and 20:6

Table 1
Characteristics of the PMMA-*co*-PHPMI copolymer synthesized in this study.

Polymer	HPMI (mol%)		P_{12}	P_{21}	M_n[a]	PDI[a]	T_g[b]
	Monomer feed	Polymer composition					(°C)
PHPMI	100	100	–	–	7950	1.06	209
PHPMI-56	82.6	56.5	0.16	0.95	10,900	1.36	212
PHPMI-50	67.9	50.7	0.31	0.90	14,200	1.58	210
PHPMI-41	50.0	41.2	0.48	0.81	19,300	1.71	198
PHPMI-28	34.6	28.5	0.64	0.70	29,100	1.55	184
PHPMI-17	22.2	17.2	0.77	0.55	38,600	1.26	163
PHPMI-10	11.7	10.0	0.88	0.37	28,200	1.35	145
PHPMI-5	5.6	5.0	0.94	0.21	37,000	1.36	135
PMMA	0	0	–	–	42,000	1.80	123

[a] : Measured by GPC analyses.
[b] : Measured by DSC analyses.

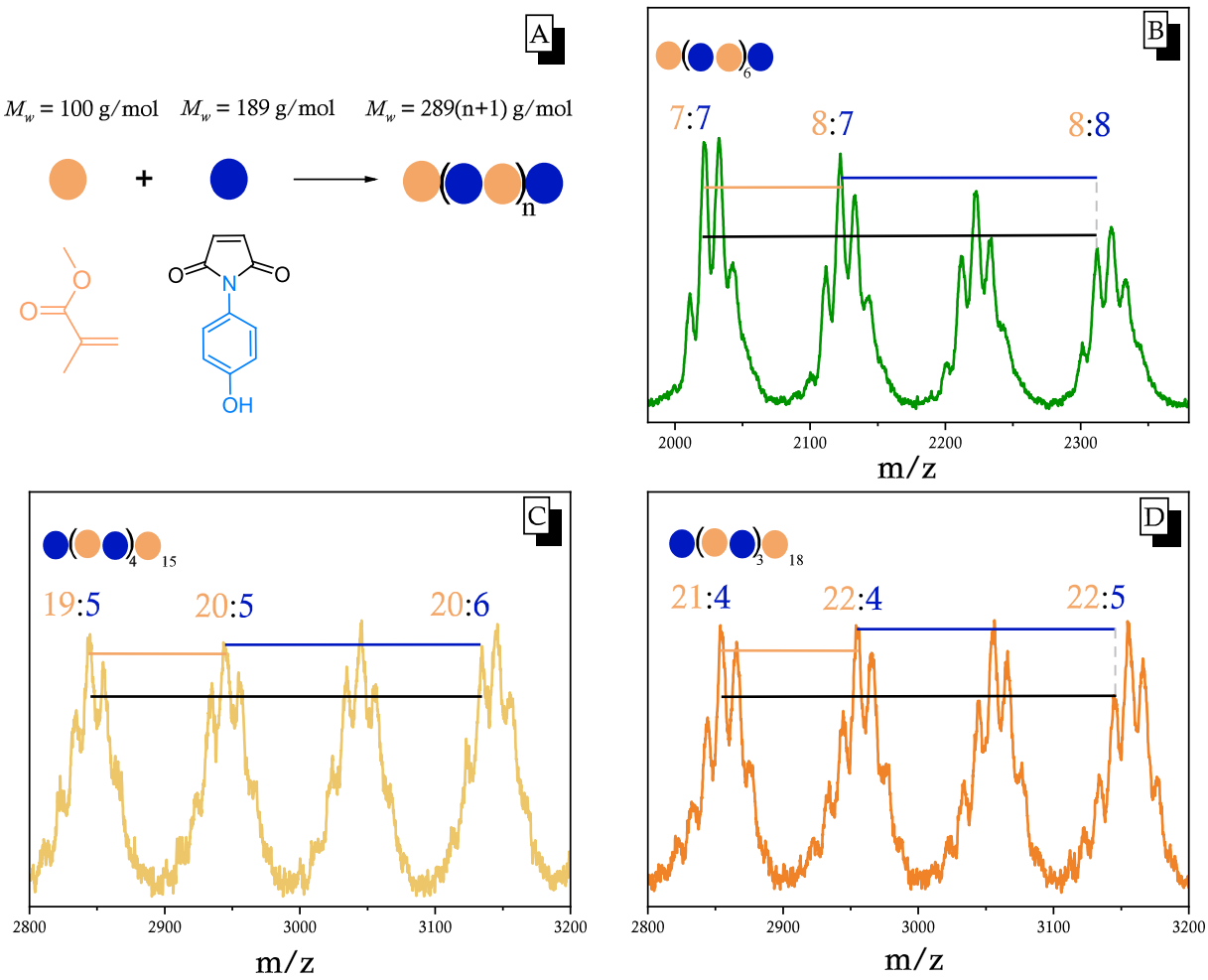

Fig. 2. (A) Chemical structures and molecular weights of the MMA and HPMI monomers. (B–D) MALDI-TOF mass spectra of (B) PHPMI-41, (C) PHPMI-17, and (D) PHPMI-10.

distributions and other peaks corresponding to ratios of MMA:HPMI of 13:8, 15:17, 21:4, and 23:3, arising from higher degrees of homo-polymerization of the MMA and HPMI units, resulting in 41% of alternating segments. Likewise, the spectrum of PHPMI-10 in Figure S2(G) reveals predominant homo-polymerization of the MMA and HPMI units, with only 30.8% of alternating segments. Therefore, the MALDI-TOF mass spectra confirmed that we had obtained partially alternating PMMA-*co*-PHPMI copolymers and Table 1 also summarizes the molecular weights and polydispersity indices (PDIs) from GPC results of these PMMA-*co*-PHPMI random copolymers.

3.2. Relationship between sequence distribution and thermal properties

Generally, the microstructure of the copolymer is affected by its sequence distribution length; the statistical relations could be predicted from their reactivity ratios. The predominantly random distribution of two monomers in a copolymerization system can be characterized as follows [40]:

$$P_{12} = 1 - P_{11} = \frac{1}{1 + r_1 X} \tag{2}$$

$$P_{21} = 1 - P_{22} = \frac{1}{1 + r_2 / X} \tag{3}$$

where X is equal to $[M_1]/[M_2]$, the composition ratio of the two feed monomers, and P_{ij} is the conditional probability of an active i radical adding to the growing j monomer to form an alternating copolymer. Herein, we defined M_1 and M_2 to be the HPMI and MMA monomers, respectively, and calculated the values of P_{12} and P_{21} (Table 1) from Eqs. (2) and (3). For instance, the microstructure of HPMI in the PHPMI-41 copolymer comprised 48% of isolated HPMI units, 25% of diads, 13% of triads, and 7% of tetrads (i.e., 7% = $P_{11}{}^3 \times P_{12} \times 100\%$). The microstructure of MMA in the PHPMI-41 copolymer comprised 81% of isolated MMA units, 15% of diads, 3% of triads, and 1% of tetrads, implying that the MMA monomer generally ended up in as isolated single MMA sequences (M_2) in these PMMA-*co*-PHPMI copolymers [11]. Intermolecular hydrogen bonding between the phenolic OH units of PHPMI and the C = O units of PMMA would be more likely to occur in such copolymers; that is, the probability P_{21} for self-association hydrogen bonding would be larger than that of pure PHPMI (P_{11}).

Fig. 3(A) presents the results of DSC thermal analyses of pure PMMA, pure PHPMI, and the various PMMA-*co*-PHPMI copolymers. Each trace revealed a single value of T_g, indicating that no macrophase separation occurred, and that the values of T_g increased upon increasing the HPMI ratio. Many attempts have been made, based on thermodynamic treatment, to modify the Fox equation for values of T_g in miscible polymer blend or copolymer. These equations can still deviate significantly for systems featuring strong intermolecular interactions, although they have been successfully applied to some blends or copolymers. The Kwei equation is generally preferred for hydrogen-bonded polymer blend or copolymer, based on its more adequate treatment at describing the composition-dependence of the values of T_g, defined as follows [41]:

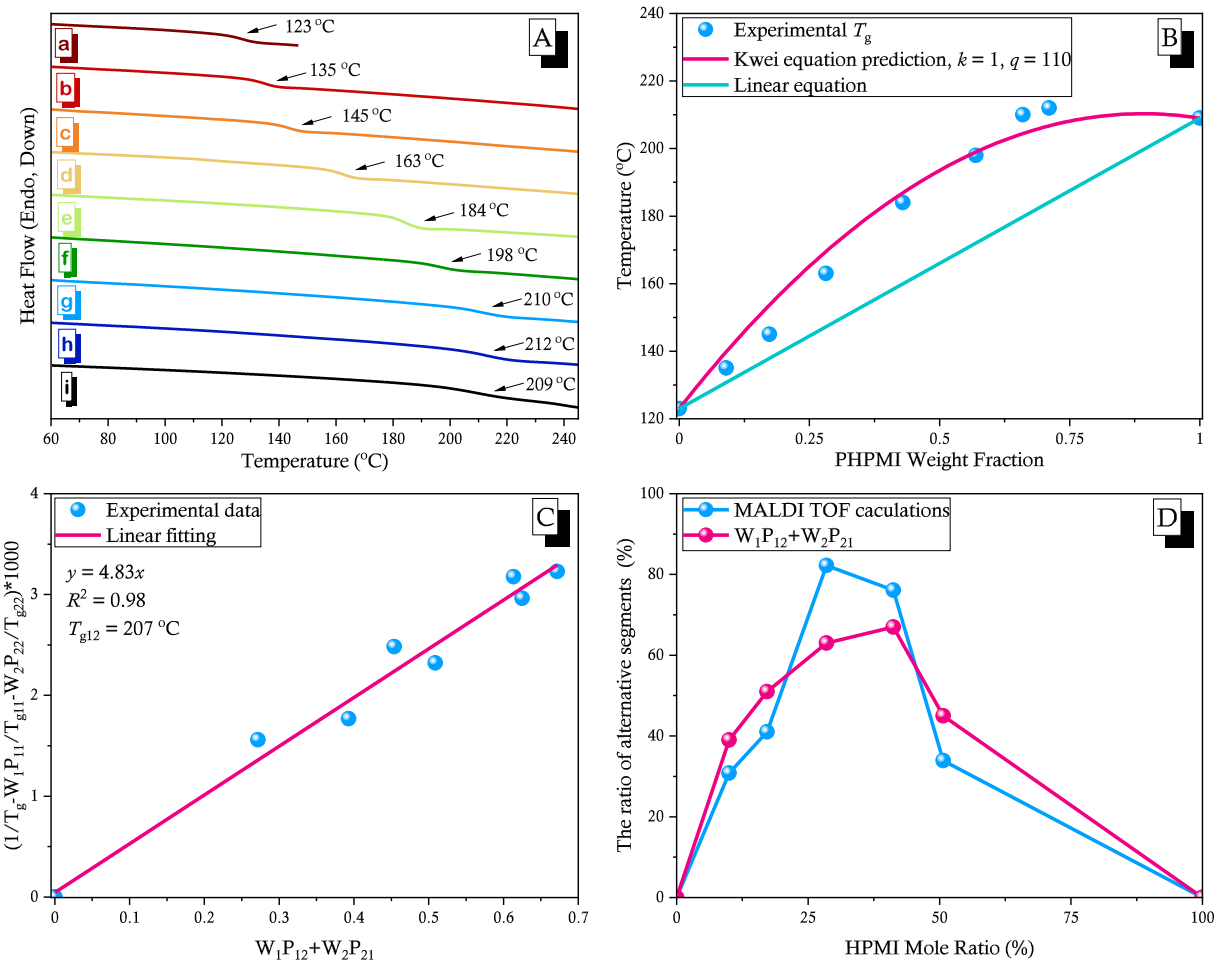

Fig. 3. (A) DSC thermal analyses of (a) PMMA, (b) PHPMI-5, (c) PHPMI-10, (d) PHPMI-17, (e) PHPMI-28, (f) PHPMI-41, (g) PHPMI-50, (h) PHPMI-56, and (i) PHPMI. (B) Values of T_g predicted by the Kwei equation. (C) Application of the linearized expression of Johnston's treatment to the PMMA-*co*-PHPMI copolymers. (D) Alternating ratio segments plotted with respect to the HPMI molar ratio.

$$T_g = \frac{W_1 T_{g1} + kW_2 T_{g2}}{W_1 + kW_2} + qW_1 W_2 \tag{4}$$

where W_1 and W_2 are weight fractions of the copolymer segments; T_{g1} and T_{g2} are the glass transition temperatures of the copolymer segments; and k and q are fitting constants. In general, q represents the strength of intermolecular hydrogen bonding in miscible polymer blends or copolymer systems. We obtained values of k and q of 1 and 110, respectively, through nonlinear least-squares fitting based on Eq. (4) in Fig. 3(B). We also found that the linear rule did not fit well for these PMMA-*co*-PHPMI copolymers. As a result, the positive value of q suggests that strong hydrogen bonding occurred between the MMA and HPMI segments. Notably, incorporating only 17.2 and 56.5 mol % of HPMI into the PMMA-*co*-PHPMI copolymers increased the value of T_g by 40 and 90 °C, relative to that of pure PMMA. The values of k and q for the PMMA-*co*-PVPh random copolymer (1 and 50, respectively) were smaller than those for the PMMA-*co*-PHPMI copolymers [20]. Unlike PHPMI, the PVPh sequences could not undergo self-association through interactions of phenolic OH and C = O units; therefore, PMMA-*co*-PVPh presumably featured a higher fraction of hydrogen-bonded C = O groups among its PMMA segments, arising from the different sequence distributions in the PMMA-*co*-PVPh and PMMA-*co*-PHPMI random copolymer systems.

We used free-volume theory to investigate the dependence of the values of T_g on the compositions of the polymer blends and copolymers [42]. Four possible sequences of diad units can be formed in copolymers derived from M_1 and M_2 monomers: P_{11}, P_{22}, P_{12}, and P_{21}. Johnston et al. expanded the Fox rule by using free-volume theory, assigning individual values of T_g to the 12/21, 11, and 22 diads, as follows [42]:

$$\frac{1}{T_g} - \frac{W_1 P_{11}}{T_{g11}} - \frac{W_2 P_{22}}{T_{g22}} = \frac{1}{T_{g12}}(W_1 P_{12} + W_2 P_{21}) \tag{5}$$

where T_g is experimental glass transition temperature of each copolymer; W_1 and W_2 are the weight fractions the copolymer segments; T_{g11} and T_{g22} are the glass transition temperatures of the pure homopolymers; and T_{g12} is the glass transition temperature of the alternating copolymer. Fig. 3(C) reveals that our experimental data could also be fitted well with a linear relationship to the Johnston equation. We obtained a T_g for the alternating copolymer (T_{g12}) of 207 °C, based on the slope of this straight line; this value is much higher than that of pure PMMA and close to that of pure PHPMI. Fig. 3(D) presents the ratios of alternating segments calculated from the MALDI-TOF mass spectra and the probabilities from statistical derivation of copolymerization. We observe similar trends in the ratios of the alternating segments, with the maximum value obtained at approximately 40 mol % of HPMI, for which the monomer feed was 50 mol %; these findings suggest a reason for the high values of T_g of our partially alternating PMMA-*co*-PHPMI copolymers. In addition, the TGA analyses were summarized in Figure S3, where the thermal decomposition temperature was increased with the increase of PHPMI compositions in PMMA-*co*-PHPMI copolymers.

3.3. FTIR spectral analyses

From the chemical structures and observed thermal analytical data,

hydrogen bonding must have been occurring in these PMMA-*co*-PHPMI copolymers. FTIR spectroscopy is a powerful tool for understanding hydrogen bonding in polymeric materials. Fig. 4(A) displays the scale-expanded FTIR spectra (3750–2750 cm^{-1}) of pure PMMA, pure PHPMI, and various PMMA-*co*-PHPMI copolymers, recorded at 120 °C. In the spectrum of pure PHPMI, signals for free OH stretching of the HPMI units appeared near 3670 cm^{-1}; the signals for OH stretching of the HPMI units involved in self-association hydrogen bonding appeared near 3300–3600 cm^{-1}, with those for self-association OH···O = C and OH···OH hydrogen bonding centered at 3445 and 3226 cm^{-1}, respectively. The intensities of the signals for free OH stretching and OH···OH self-association of the HPMI units decreased upon increasing the composition of PMMA in the PMMA-*co*-PHPMI copolymers; furthermore, the signal for OH···OH self-association shifted to higher wavenumber (to ca. 3445 cm^{-1}), corresponding to the signal for intermolecular OH···O = C hydrogen bonding between the C = O units of PMMA and the OH units of PHPMI. Fig. 4(B) displays the signals for C = O stretching in the range from 1800 to 1660 cm^{-1} in the corresponding FTIR spectra recorded at 120 °C. Because the PMMA and PHPMI segments both featured C = O groups in their repeat units we expected to observe signals for at least four C = O units in the spectra of our PMMA-*co*-PHPMI copolymers: for symmetric (hydrogen-bonded) and asymmetric HPMI units at 1702 and 1776 cm^{-1}, respectively, and for free and hydrogen-bonded PMMA units at 1730 and 1713 cm^{-1}, respectively. The signals for the C = O units shifted to lower wavenumbers upon increasing the HPMI content in the copolymers [Fig. 4(B)]. Fig. 4(C) and 4(D) present selected curve fitting data for these four peaks in the spectra of PHPMI-50 and PHPMI-10; Table 2 summarizes area fraction of each C = O unit. For the PMMA-*co*-PHPMI copolymers, the area fraction for the self-association of hydrogen-bonded C = O groups of the HPMI segments decreased upon increasing the PMMA composition, while the fraction of hydrogen-bonded C = O groups of the PMMA units increased upon increasing the PHPMI compositions, suggesting that interactions existed between the C = O groups of the PMMA segments and the OH

Table 2
Curve fitting data for the C = O and amide groups in the FTIR spectra of the PMMA-*co*-PHPMI copolymers.

	Free C = O of PHPMI		Free C = O of PMMA		H-Bonded C = O of PMMA		Fraction of H-Bonded C = O of PMMA
	ν (cm^{-1})	A_f (%)	ν (cm^{-1})	A_f (%)	ν (cm^{-1})	A_f (%)	$f_b^{C=O}$
PHPMI	1702	100	–	–	–	–	–
PHPMI-56	1702	68	1730	11	1713	17	0.61
PHPMI-50	1703	63	1730	13	1713	19	0.59
PHPMI-41	1704	51	1731	24	1713	21	0.47
PHPMI-28	1705	43	1732	30	1714	22	0.42
PHPMI-17	1706	31	1733	42	1714	25	0.37
PHPMI-10	1707	13	1734	55	1716	28	0.34
PHPMI-5	1708	2	1735	63	1717	30	0.32
PMMA	–	–	1730	100	–	–	–

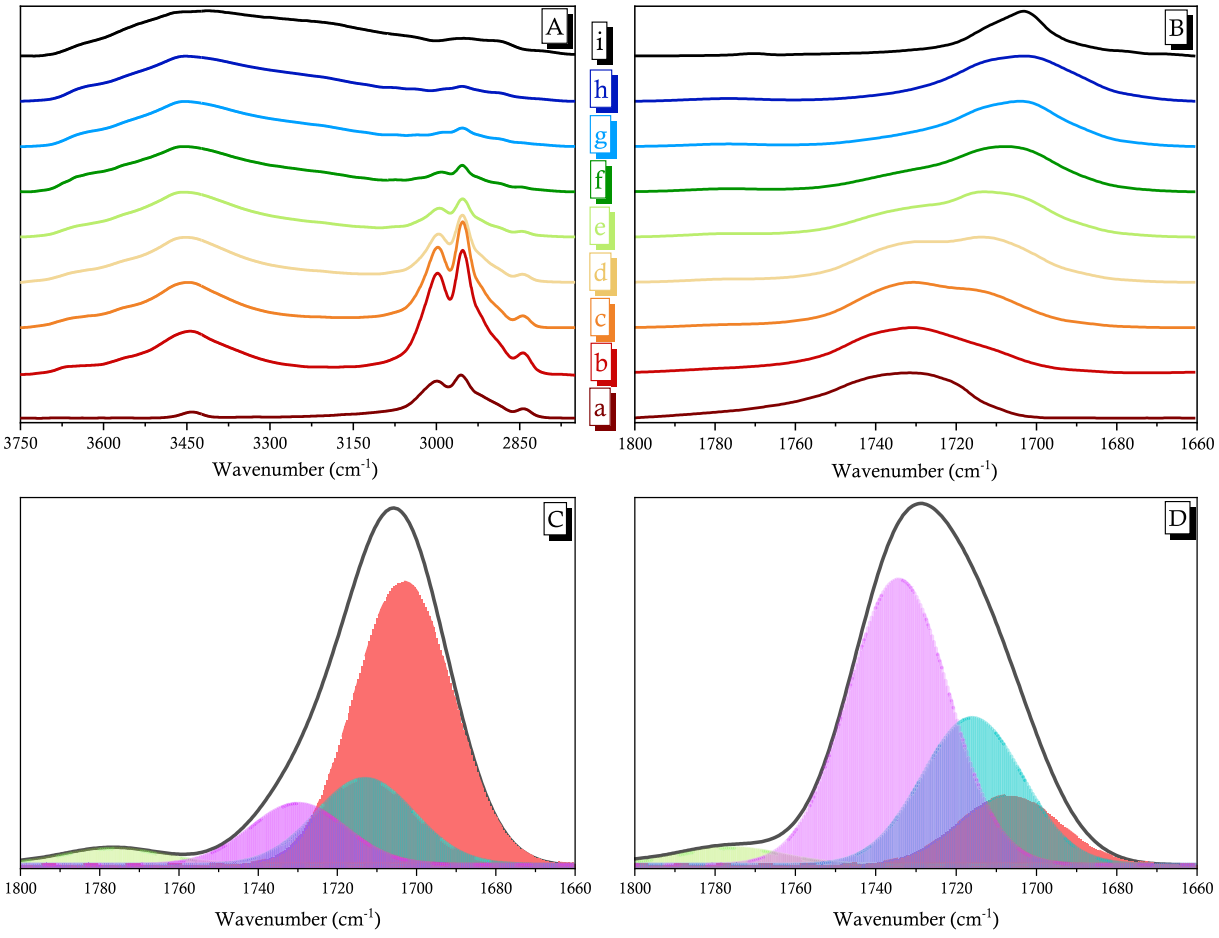

Fig. 4. (A) OH and (B) C = O stretching regions of the FTIR spectra of (a) PMMA, (b) PHPMI-5, (c) PHPMI-10, (d) PHPMI-17, (e) PHPMI-28, (f) PHPMI-41, (g) PHPMI-50, (h) PHPMI-56, and (i) PHPMI. (C, D) FTIR spectral curve fitting data for the C = O absorptions of (C) PHPMI-50 and (D) PHPMI-10.

groups of the PHPMI segments. As a result, these copolymers featured enhanced values of T_g.

3.4. Solid state NMR spectral analyses

Solid state NMR spectra provided insight into the hydrogen bonding and domain sizes of these PMMA-*co*-PHPMI copolymers. Fig. 5(A) and 5 (B) present ^{13}C solid state NMR spectra of pure PMMA, pure PHPMI, and our PMMA-*co*-PHPMI copolymers. The signal for the imide carbon nuclei of pure PHPMI appeared at δ 177.1 ppm and that of the C = O carbon nuclei of PMMA appeared at δ 177.9 ppm; the signal for the phenolic OH carbon nuclei of pure PHPMI appeared at δ 157.1 ppm. Experimental and simulated data confirmed the presence of hydrogen bonding in the PMMA-*co*-PHPMI copolymers, based on solid state NMR spectral analyses [43]. The simulated spectra of each copolymer, displayed on the right-hand side in Fig. 5(A) and 5(B), were obtained simply by summing of experimental ^{13}C NMR spectra of the pure PMMA and pure PHPMI at the relevant molar ratios. The experimental spectra of the PMMA-*co*-PHPMI copolymers were significantly different from the simulated spectra. Complicated and broad signals in the experimental spectra suggested that hydrogen bonding occurred between the C = O units of PMMA and the phenolic OH units of PHPMI. Fig. 5(C) indicates that the full widths at half maximum (FWHMs) of most of the copolymers were larger than that of the pure PHPMI, and that the signal of the C = O groups of PMMA shifted upfield upon increasing the composition of HPMI in the copolymers, confirming that interactions occurred between these two segments [Fig. 5(D)-(a)]. Nevertheless, the signal for the C = O groups of the PMMA units slightly shifted to higher field upon increasing the HPMI content, with a slower increase in the FWHM of the C = O groups; correspondingly, the signal of the phenolic COH units of PHPMI shifted downfield, as expected. The situation is consistent with the phenolic OH units of PHPMI interacting not only with the C = O groups of PMMA but also through self-association with the imide C = O units of PHPMI, as displayed in Fig. 5(D)-(b), consistent with the conclusions drawn from the FTIR spectral analyses.

3.5. Spin–Lattice relaxation times in the rotating frame [$T_{1\rho}$(H)]

The domain sizes and molecular mobilities in hydrogen-bonded blends or copolymers can be investigated in terms of the values of $T_{1\rho}$(H) in the rotating frame [44]; these values can be calculated from.

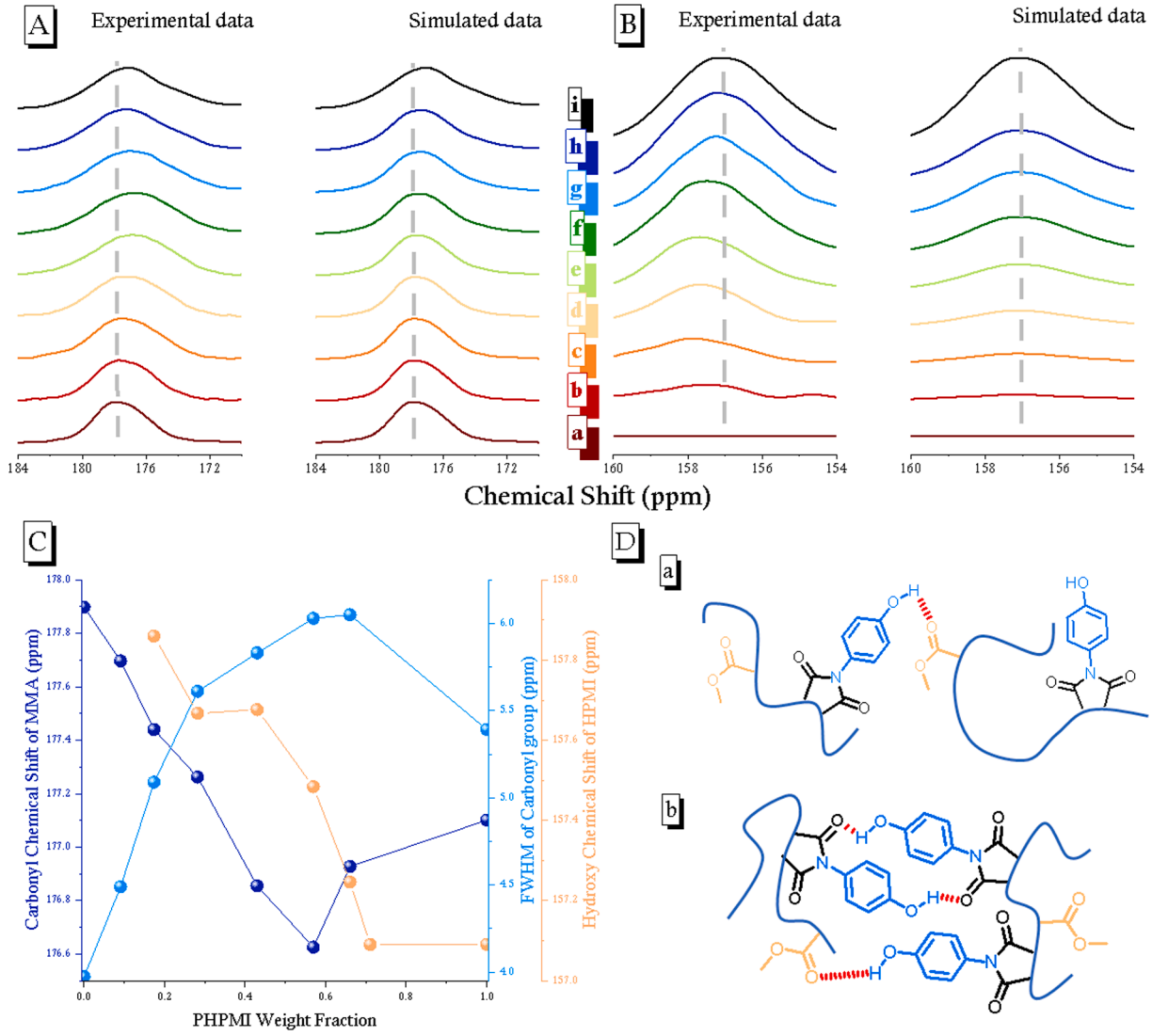

Fig. 5. (A) C = O and (B) COH nuclei in the ^{13}C solid state CP/MAS NMR spectra of (a) PMMA, (b) PHPMI-5, (c) PHPMI-10, (d) PHPMI-17, (e) PHPMI-28, (f) PHPMI-41, (g) PHPMI-50, (h) PHPMI-56, and (i) PHPMI. (C) Chemical shifts and FWHMs for PMMA-*co*-PHPMI copolymers prepared with various PHPMI contents. (D) (a) Intermolecular hydrogen bonding between PHPMI and PMMA and (b) intermolecular hydrogen bonding through self-association of PHPMI and intermolecular hydrogen bonding between PHPMI and PMMA.

$$M_\tau = M_0 \exp[-\tau/T_{1\rho}(H)] \quad (6)$$

where τ is the spin-lock time and M_0 and M_τ are the intensities of the peaks measured experimentally initially and after τ seconds, respectively. Fig. 6(A) displays plots of $\ln(M_\tau/M_0)$ with respect to τ for the C = O units at δ 177 ppm for all copolymer compositions where the experimental data provided a single exponential decay function. Based on the slope of the plot in Eq. (6), we calculated a single value of $T_{1\rho}$(H) in the copolymer, indicating that the miscibility dimensions of copolymer were less than 2–3 nm, based on the one-dimensional diffusion equation and the average diffusive path length, as follows [44]:

$$L = \sqrt{6DT_{1\rho}(H)}$$

where D is the effective spin-diffusion coefficient, which depends on the average distance among two protons as well as their dipolar interactions. This PMMA-*co*-PHPMI copolymer could be considered as one component and should be miscible, based on thermodynamic considerations of such a covalently bonded system. The average proton-relaxation rate of a copolymer or miscible blend can be predicted through linear additivity of the relaxation rate model [44]:

$$\frac{1}{T_{1\rho}(H)} = \frac{N_A M_A}{N_T}\left(\frac{1}{T_{1\rho}(H)_A}\right) + \frac{N_B M_B}{N_T}\left(\frac{1}{T_{1\rho}(H)_B}\right) \quad (8)$$

where A and B represent each component of the copolymer segments; M_i is the mole fraction of each component; N_i is the number of protons of each component; and

$N_T = N_A M_A + N_B M_B$.

$T_{1\rho}(H)_A$ and $T_{1\rho}(H)_B$ represent the relaxation rates of components A and B, respectively. Fig. 6(B) plots the values of $T_{1\rho}$(H) with respect to the PHPMI mole fraction, determined from experimental and calculated data based on Eq. (8). The experimental relaxation rate for each copolymer composition deviated negatively from the calculated value based on Eq. (8), implying significant changes relative to prediction in the free volume and density for each copolymer [45]. This finding indicates that the segmental motions of these copolymers were altered significantly, such that these copolymers featuring strong hydrogen bonding exhibited rigid behavior. In contrast, we observed macrophase separation when blending the PHPMI homopolymer with the PMMA homopolymer [Fig. 6(C) and 6(D)-(c)]. Fig. 6(C)-(e) reveals that, at various ratios, the PMMA/PHPMI homopolymer blends provided the two individual values of T_g of PMMA and PHPMI, suggesting that macrophase separation occurred in these binary blends. Consequently, we needed to copolymerize MMA and HPMI to achieve good miscibility and to increase their values of T_g based on a composition heterogeneity effect [46].

4. Conclusions

Strong hydrogen bonding in PMMA-*co*-PHPMI copolymers featuring a partially alternating sequence distribution in the main chain leads to a position deviation in the value of T_g based on the linear rule. FTIR and solid state NMR spectroscopy confirmed that such hydrogen bonding was occurring in these copolymer systems. We obtained single values of $T_{1\rho}$(H) for all of the copolymers; these values were lower than those predicted by the linear rule, suggesting that the degree of homogeneity

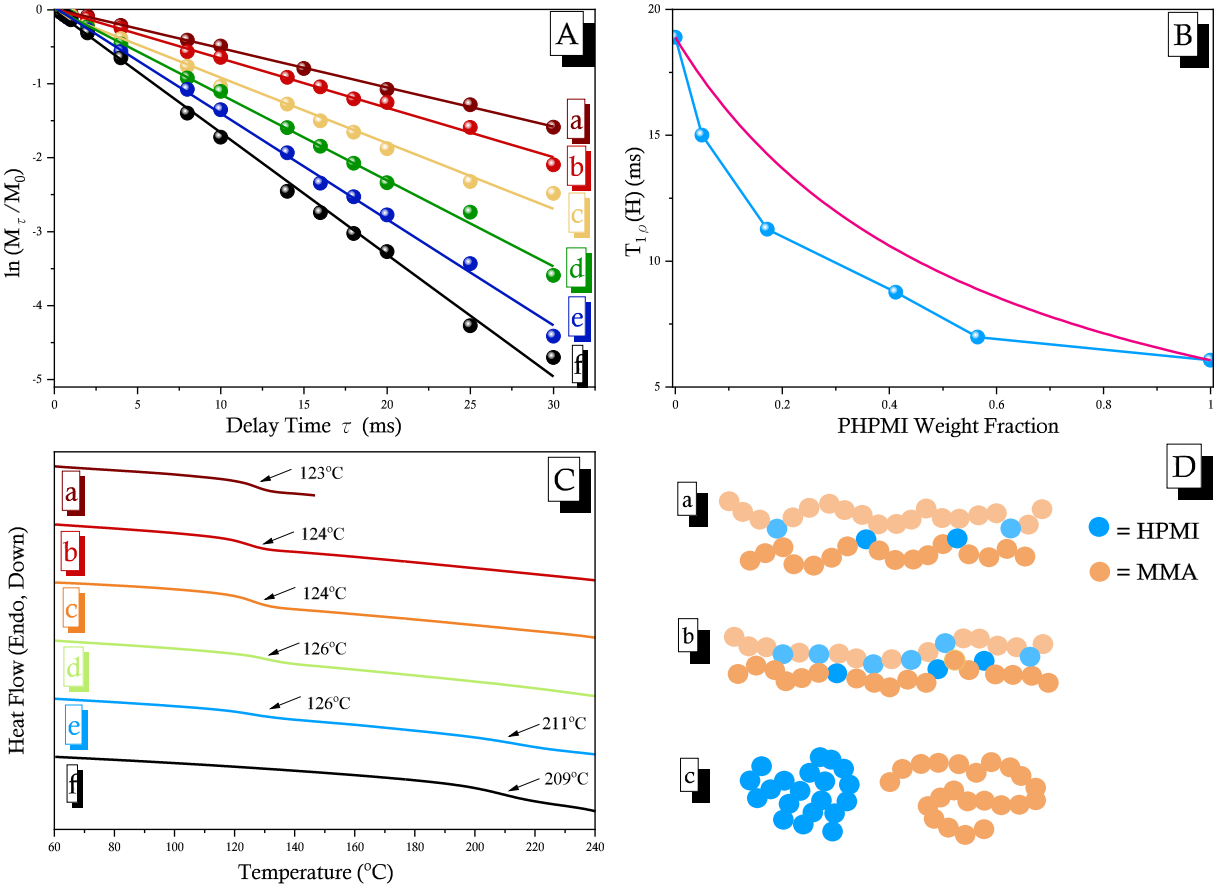

Fig. 6. (A) Semi-logarithmic plots of the magnetization intensities of 177 ppm with respect to the delay time for PMMA-*co*-PHPMI copolymers at a contact time of 1 ms for (a) PMMA, (b) PHPMI-5, (c) PHPMI-17, (d) PHPMI-41, (e) PHPMI-56, and (f) PHPMI. (B) Plots of $T_{1\rho}$(H) calculated from Eq. (8) with respect to the PHPMI content of the PMMA-*co*-PHPMI copolymers. (C) DSC analyses of PMMA/PHPMI binary blends: (a) pure PMMA, (b) 95/5, (c) 90/10, (d) 72/28, (e) 50/50, and (f) pure PHPMI. (D) Possible chain behavior of (a, b) PMMA-*co*-PHPMI copolymers with (a) low and (b) high HPMI contents and (c) binary PMMA/PHPMI blends.

was less than 2–3 nm and that the free volume was lower than the prediction in these hydrogen-bonded PMMA-*co*-PHPMI copolymers. As a result, significant enhancement in the value of T_g of PMMA can be obtained through random copolymerization with partially alternating sequence distributions of hydrogen-bonded donor HPMI units, even though the resulting copolymers feature self-associating hydrogen-bonded units.

CRediT authorship contribution statement

Wei-Ting Du: Data curation, Writing – original draft. **Shiao-Wei Kuo:** Supervision.

Declaration of Competing Interest

The authors declare that they have no known competing financial interests or personal relationships that could have appeared to influence the work reported in this paper.

Acknowledgments

This study was supported financially by the Ministry of Science and Technology, Taiwan, under contracts MOST 108-2221-E-110-014-MY3.

Appendix A. Supplementary material

Supplementary data to this article can be found online at https://doi.org/10.1016/j.eurpolymj.2022.111165.

REFERENCES

[1] C. Pavlou, M.G.P. Carbone, A.C. Manikas, G. Trakakis, C. Koral, G. Papari, A. Andreone, C. Galiotis, Effective EMI shielding behaviour of thin graphene/PMMA nanolaminates in the THz range, Nat. Commun. 12 (2021) 4655.
[2] R.J. Sengwa, P. Dhatarwal, Polymer nanocomposites comprising PMMA matrix and ZnO, SnO_2, and TiO_2 nanofillers: A comparative study of structural, optical, and dielectric properties for multifunctional technological applications, Optical Mater. 113 (2021), 110837.
[3] T.-J. Wang, N.R. Barveen, Z.-Y. Liu, C.-H. Chen, M.-H. Chou, Transparent, Flexible Plasmonic Ag NP/PMMA Substrates Using Chemically Patterned Ferroelectric Crystals for Detecting Pesticides on Curved Surfaces, ACS Appl. Mater. Interfaces 13 (29) (2021) 34910–34922.
[4] T.T. Ava, H.J. Jeong, H.M. Yu, K.N. Lee, T.M. Fattah, M.S. Jeong, G. Namkoong, Role of PMMA to make $MAPbI_3$ grain boundary heat-resistant, Appl. Surface Sci. 558 (2021), 149852.
[5] S.-L. Yeh, C.-Y. Zhu, S.-W. Kuo, Transparent Heat-Resistant PMMA Copolymers for Packing Light-Emitting Diode Materials, Polymers 7 (8) (2015) 1379–1388.
[6] R. Whitfield, K. Parkatzidis, N.P. Truong, T. Junkers, A. Anastasaki, Tailoring Polymer Dispersity by RAFT Polymerization: A Versatile Approach, Chem 6 (2020) 1340.
[7] K. Fila, M. Goliszek, B. Podkościelna, M. Podgórski, Polymer side-chain modification in methacrylate and styrene copolymers through thiol-thioester dynamic exchange, Eur. Polym. J. 136 (2020), 109918.
[8] F.E. Caligiore, D. Nazzari, E. Cianci, K. Sparnacci, M. Laus, M. Perego, G. Seguini, Effect of the density of reactive sites in P(S-r-MMA) film during Al_2O_3 growth by sequential infiltration synthesis, Adv. Mater. Interfaces 6 (2019) 1900503.
[9] J. Park, M.J. Baek, H.W. Choi, H.S. Kim, D.W. Lee, Development of Poly(methyl methacrylate)-Based Copolymers with Improved Heat Resistance and Reduced Moisture Absorption, Langmuir 35 (2019) 15880.
[10] Y. Li, H. Guo, Crosslinked poly(methyl methacrylate) with perfluorocyclobutyl aryl ether moiety as crosslinking unit: thermally stable polymer with high glass transition temperature, RSC Adv. 10 (2020) 1981–1988.
[11] F. Atabaki, A. Abdolmaleki, A. Barati, Free radical copolymerization of methyl methacrylate and N-2-methyl-4-nitro-phenylmaleimide: Improvement in the T_g of PMMA, Colloid Polym. Sci. 294 (2016) 455–462.
[12] H. Teng, L. Yang, F. Mikes, Y. Koike, Y. Okamoto, Property modification of poly (methyl methacrylate) through copolymerization with fluorinated aryl methacrylate monomers, Polym. Adv. Technol. 18 (6) (2007) 453–457.
[13] S. Dong, Q. Wang, Y. Wei, Z. Zhang, Study on the synthesis of heat-resistant PMMA, J. Appl. Polym. Sci. 72 (1999) 1335–1339.
[14] A. Mishra, T.J.M. Sinha, V. Choudhary, Methyl methacrylate–N-chlorophenyl maleimide copolymers: Effect of structure on properties, J. Appl. Polym. Sci. 68 (4) (1998) 527–534.
[15] S.-W. Kuo, H.-C. Kao, F.-C. Chang, Thermal behavior and specific interaction in high glass transition temperature PMMA copolymer, Polymer 44 (22) (2003) 6873–6882.
[16] J.-K. Chen, S.-W. Kuo, H.-C. Kao, F.-C. Chang, Thermal properties, specific interactions, and surface energies of PMMA terpolymers having high glass transition temperatures and low moisture absorptions, Polymer 46 (7) (2005) 2354–2364.
[17] C.-T. Lin, S.-W. Kuo, C.-F. Huang, F.-C. Chang, Glass transition temperature enhancement of PMMA through copolymerization with PMAAM and PTCM mediated by hydrogen bonding, Polymer 51 (4) (2010) 883–889.
[18] S.-W. Kuo, Hydrogen bonding interactions in polymer/polyhedral oligomeric silsesquioxane nanomaterials, J Polym Res 29 (2) (2022), https://doi.org/10.1007/s10965-021-02885-4.
[19] P.G. De Gennes, Scaling Concept in Polymer Physics, Cornell University Press, 1979.
[20] C.-L. Lin, W.-C. Chen, C.-S. Liao, Y.-C. Su, C.-F. Huang, S.-W. Kuo, F.-C. Chang, Sequence distribution and polydispersity index affect the hydrogen-bonding strength of poly (vinylphenol-co-methyl methacrylate) copolymers, Macromolecules 38 (15) (2005) 6435–6444.
[21] T.-C. Tseng, S.-W. Kuo, Hydrogen-Bonding Strength Influences Hierarchical Self-Assembled Structures in Unusual Miscible/Immiscible Diblock Copolymer Blends, Macromolecules 51 (16) (2018) 6451–6459.
[22] T.-C. Tseng, S.-W. Kuo, Hydrogen bonding induces unusual self-assembled structures from mixtures of two miscible disordered diblock copolymers, Eur. Polym. J. 116 (2019) 361–369.
[23] S. W. Kuo, Hydrogen Bonding Mediated Self-Assembled Structures from Block Copolymer Mixtures to Mesoporous Materials, Polym. Inter. (2022) doi.org/10.1002/pi.6264.
[24] G. Odian, Principles of Polymerization, Wiley, New York (2004).
[25] W.T. Du, E.A. Orabi, M.G. Mohamed, S.W. Kuo, Inter/intramolecular hydrogen bonding mediate miscible blend formation between near-perfect alternating Poly (styrene-alt-hydroxyphenylmaleimide) copolymers and Poly(vinyl pyrrolidone), Polymer 219 (2021), 123542.
[26] M. Tang, R. Xu, R. Zhang, S.J. Bai, G. Huang, Y.X. Xu, Bioinspired strategy to tune viscoelastic response of thermoplastic polyisoprene by retarding the dissociation of hydrogen bonding, Polymer 212 (2021), 123272.
[27] I. Helmers, G. Ghosh, R.Q. Albuquerque, G. Fernández, Pathway and Length Control of Supramolecular Polymers in Aqueous Media via a Hydrogen Bonding Lock, Angew Chem. Inter. Ed. 60 (8) (2021) 4368–4376.
[28] A. F. M. EL-Mahdy, T. C. Yu, S. W. Kuo, Synthesis of multiple heteroatom–doped mesoporous carbon/silica composites for supercapacitors, Chem. Eng. J. 414 (2021) 128796.
[29] A.F.M. EL-Mahdy, T.C. Yu, M.G. Mohamed, S.-W. Kuo, Secondary Structures of Polypeptide-Based Diblock Copolymers Influence the Microphase Separation of Templates for the Fabrication of Microporous Carbons, Macromolecules 54 (2) (2021) 1030–1042.
[30] M.G. Mohamed, E.C. Atayde, B.M. Matsagar, J. Na, Y. Yamauchi, K.-W. Wu, S.-W. Kuo, Construction Hierarchically Mesoporous/Microporous Materials Based on Block Copolymer and Covalent Organic Framework, J. Taiwan Inst. Chem. Eng. 112 (2020) 180–192.
[31] A. F. M. EL-Mahdy, T. E. Liu, S. W. Kuo, Direct synthesis of nitrogen-doped mesoporous carbons from triazine-functionalized resol for CO_2 uptake and highly efficient removal of dyes, J. Hazard. Mater. 391 (2020) 122163.
[32] M.G. Mohamed, S.-W. Kuo, Crown Ether-Functionalized Polybenzoxazine for Metal Ion Adsorption, Macromolecules 53 (7) (2020) 2420–2429.
[33] M.G. Mohamed, S.W. Kuo, Functional silica and carbon nanocomposites based on polybenzoxazines, Macromol. Chem. Phys. 220 (2019) 1800306.
[34] M.G. Mohamed, S.W. Kuo, Functional Polyimide/Polyhedral Oligomeric Silsesquioxane Nanocomposites, Polymers 11 (2019) 26.
[35] S. Zhang, Q. Ran, Q. Fu, Y.i. Gu, Preparation of Transparent and Flexible Shape Memory Polybenzoxazine Film through Chemical Structure Manipulation and Hydrogen Bonding Control, Macromolecules 51 (17) (2018) 6561–6570.
[36] S.W. Kuo, F.C. Chang, Effect of copolymer composition on the miscibility of poly (styrene-co-acetoxystyrene) with phenolic resin, Polymer 42 (24) (2001) 9843–9848.
[37] L.R. Hutchings, P.P. Brooks, J.A. Mosely, S. Sevinc, Monomer Sequence Control via Living Anionic Copolymerization: Synthesis of Alternating, Statistical, and Telechelic Copolymers and Sequence Analysis by MALDI ToF Mass Spectrometry, Macromolecules 48 (2015) 610–628.
[38] D.C. Schriemer, L. Li, Detection of High Molecular Weight Narrow Polydisperse Polymers up to 1.5 Million Daltons by MALDI Mass Spectrometry, Anal. Chem. 68 (17) (1996) 2721–2725.
[39] M.G. Mohamed, K.C. Hsu, J.L. Hong, S.W. Kuo, Unexpected fluorescence from maleimide-containing polyhedral oligomeric silsesquioxanes: nanoparticle and sequence distribution analyses of polystyrene-based alternating copolymers, Polym. Chem. 7 (2016) 135–145.
[40] J. San Roman, E.L. Madruga, M.A. del Puerto, Radical copolymerization of acrylic monomers. IV. Effect of substituents on the radical polymerization and copolymerization of phenyl acrylates, J. Polym. Sci., Polym. Chem. Ed. 21 (1983) 691.
[41] T.K. Kwei, The effect of hydrogen bonding on the glass transition temperatures of polymer mixtures, J. Polym. Sci.: Polym. Lett. Ed. 22 (6) (1984) 307–313.
[42] S.W. Kuo, Hydrogen Bonding in Polymeric Materials; John Wiley & Sons: Hoboken, NJ, USA, 2018.

[43] A. Asano, M. Eguchi, M. Shimizu, T. Kurotsu, Miscibility and Molecular Motion of PMAA/PVAc Blends Investigated by High-Resolution Solid-State CPMAS ^{13}C NMR, Macromolecules 35 (2002) 8819.
[44] C. Lau, Y. Mi, A study of blending and complexation of poly (acrylic acid)/poly (vinyl pyrrolidone), Polymer 43 (2002) 823.
[45] S.-W. Kuo, P.-H. Tung, F.-C. Chang, Syntheses and the study of strongly hydrogen-bonded poly (vinylphenol-b-vinylpyridine) diblock copolymer through anionic polymerization, Macromolecules 39 (26) (2006) 9388–9395.
[46] M.M. Coleman, Y. Xu, P.C. Painter, Compositional heterogeneities in hydrogen-bonded polymer blends: infrared spectroscopic results, Macromolecules 27 (1994) 127–134.